



First Imaging Observation of Standing Slow Wave in Coronal Fan Loops

V. Pant¹, A. Tiwari^{1,2}, D. Yuan³, and D. Banerjee^{1,4}

¹Indian Institute of Astrophysics, Bangalore 560 034, India

²Northumbria University, Newcastle Upon Tyne NE1 8ST, UK

³Institute of Space Science and Applied Technology, Harbin Institute of Technology, Shenzhen 518000, China

⁴Center of Excellence in Space Sciences, IISER, Kolkata, India

Received 2017 July 31; revised 2017 August 22; accepted 2017 August 22; published 2017 September 14

Abstract

We observe intensity oscillations along coronal fan loops associated with the active region AR 11428. The intensity oscillations were triggered by blast waves that were generated due to X-class flares in the distant active region AR 11429. To characterize the nature of oscillations, we created time–distance maps along the fan loops and noted that the intensity oscillations at two ends of the loops were out of phase. As we move along the fan loop, the amplitude of the oscillations first decreased and then increased. The out-of-phase nature together with the amplitude variation along the loop implies that these oscillations are very likely to be standing waves. The period of the oscillations is estimated to be ~ 27 minutes, damping time to be ~ 45 minutes, and phase velocity projected in the plane of sky to be $\sim 65\text{--}83\text{ km s}^{-1}$. The projected phase speeds were in the range of the acoustic speed of coronal plasma at about 0.6 MK, which further indicates that these are slow waves. To the best of our knowledge, this is the first report on the existence of the standing slow waves in non-flaring fan loops.

Key words: Sun: corona – Sun: oscillations – Sun: UV radiation

Supporting material: animations

1. Introduction

Magnetohydrodynamic (MHD) waves are ubiquitous in the solar corona. With the advent of modern space-based instruments, different types of wave modes have been observed in the past decade. Slow MHD modes (compressional waves) were first observed in the polar coronal holes using the UltraViolet Coronagraph Spectrometer (UVCS) by Ofman et al. (1997). Later, DeForest & Gurman (1998) and Ofman et al. (1999) reported propagating intensity disturbances (PDs) in polar plumes using the Extreme-ultraviolet Imaging Telescope (EIT) on board the *Solar and Heliospheric Observatory* (SOHO). Recently, several authors have reported that small-scale jets and spicules at the transition region and chromosphere are associated with PDs seen in polar plumes and polar coronal holes (Jiao et al. 2015; Pant et al. 2015; Samanta et al. 2015; Bryans et al. 2016; Yuan et al. 2016). Reflections of propagating slow waves were also reported in hot and flaring coronal loops using Atmospheric Imaging Assembly (AIA; Kumar et al. 2013, 2015) and X-Ray Telescope (XRT; Mandal et al. 2016) observations. The authors have reported that these waves are triggered by the flares at the footpoint of the coronal loops. Recently, Fang et al. (2015) have modeled the reflective slow mode in flaring loops using 2.5D MHD simulations in synthetic 131 Å emission images.

Apart from propagating slow waves, flare-excited standing slow waves have also been observed in hot and flaring coronal loops. Oscillations in Doppler velocity, detected in Fe XIX, were reported in hot flaring coronal loops using the Solar Ultraviolet Measurements of Emitted Radiation (SUMER)/SOHO and Solar X-Ray Telescope (SXT)/Yokoh (Wang et al. 2002). The time period of oscillations was found to be 14–18 minutes. These oscillations were interpreted as slow standing modes. Wang et al. (2003a, 2003b) have performed statistical studies of slow standing modes in several hot coronal loops and post-flare loops, respectively. They have reported a

$\pi/2$ phase shift between Doppler velocities and line intensities of Fe XIX and Fe XXI emission lines (formation $T > 6$ MK), which is the signature of a standing slow mode (see also Wang 2011; Yuan et al. 2015).

The standing slow modes are believed to be triggered by an impulsive flare, which causes asymmetric heating at one footpoint of the coronal loop (Wang et al. 2005). However, Tsiklauri et al. (2004) performed a numerical study of the longitudinal oscillations and reported that the excitation of standing oscillations is independent of the location of the impulsive heating in the loop. Taroyan et al. (2005, 2007) have performed 1D hydrodynamic simulations of standing slow modes and showed that slow standing waves can be triggered by impulsive footpoint heating as well. Taroyan et al. (2007) and Taroyan & Bradshaw (2008) have constructed a 1D hydrodynamic loop model to study and distinguish between standing and propagating slow oscillations in hot and cool coronal loops. They have reported that the phase of the intensity of the oscillation continuously changes with time due to heating and cooling of loops. Yuan et al. (2015) have performed forward modeling of standing slow modes in hot flaring coronal loops ($T > 6$ MK) and studied their imaging and spectroscopic signatures. The authors have reported that the amplitude of the oscillations along the loop should vary depending on the mode of the oscillations.

Slow standing waves are found to be strongly damped. Ofman & Wang (2002) used a 1D MHD model to study damped standing slow oscillations. The strong damping was attributed to large thermal conduction that depends on the temperature of the loops. Recently, Wang et al. (2015) observed standing slow modes in hot coronal loops using AIA 94 Å observations and reported that the thermal conduction, which is believed to damp the standing oscillations, is suppressed in hot coronal loops. Until today, standing slow modes have been observed exclusively in hot coronal loops. A very limited number of standing slow mode waves were detected by imaging observations. In this Letter, we report the evidence of standing slow waves in cool fan loops. The

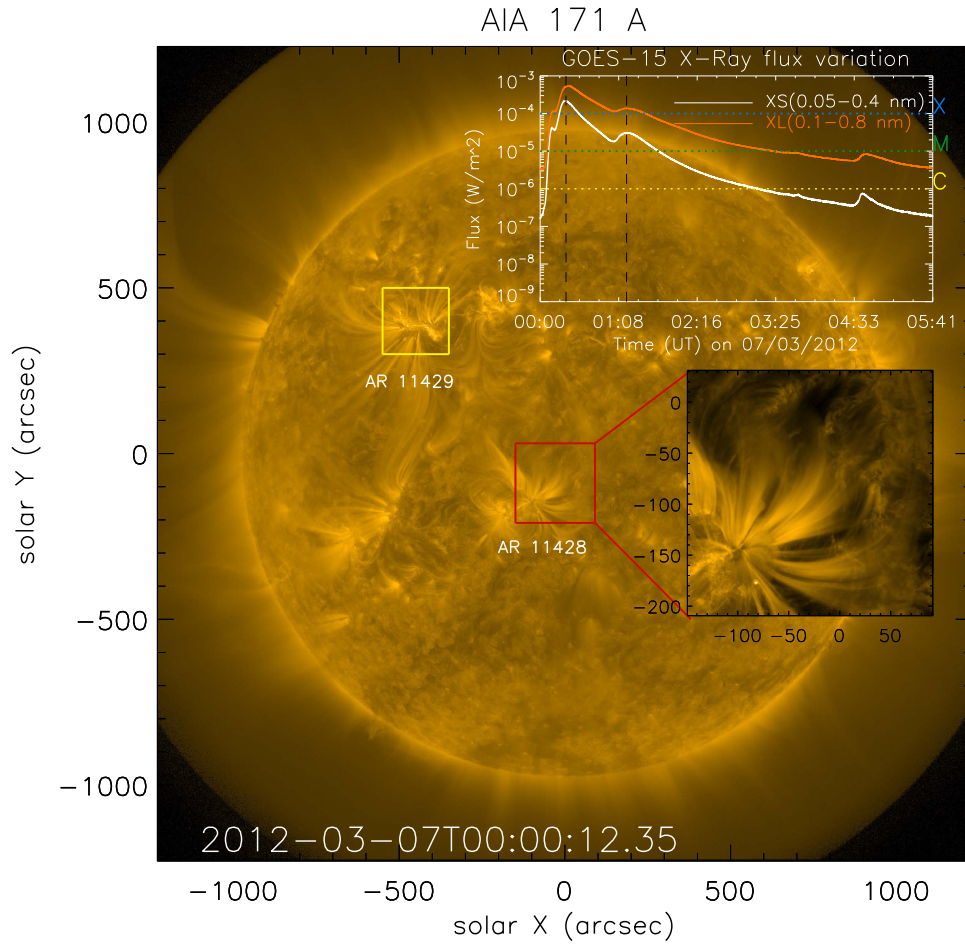


Figure 1. Full disk image of the Sun at AIA 171 Å. Red and yellow boxes represent the location of active regions AR 11428 and 11429, respectively. Region of interest (ROI) that is used for further analysis is enclosed in the red box. *GOES* X-ray flux variation is overlotted in the figure. Curves in orange and white represent the flux corresponding to two passbands, i.e., 0.1–0.8 nm and 0.05–0.4 nm, respectively. Two vertical dashed lines in black represent the timings of the peak of the *GOES* X-ray flux relevant for this study.

Letter is organized as follows. In Section 2, we describe the data processing used for this study. In Section 3, we describe the method of analysis, which is followed by a discussion and conclusions in Section 4.

2. Observations

On 2012 March 7, a group of fan loops were observed near the active region AR 11428 (see Figure 1). Two X-class flares were detected consecutively at a distant active region, AR 11429 to the northwest of AR 11428. The approximate distance between AR 11428 and AR 11429 is about 455 Mm. The *Geostationary Operational Environmental Satellite system (GOES)* X-ray emission (inset in Figure 1) exhibits the evolution of the flares. The X-ray flux at two channels peaked at 00:22 UT and 01:13 UT, respectively. The strength of two peaks corresponds to the fluxes of X5 and X1 classes, respectively. Both the X5 and X1 flares originated from AR 11429, and the associated energy pulses reach AR 11428 at 00:27 UT and 01:15 UT, respectively. The fan loops were initially driven to move transversely, and subsequently, the intensity perturbations along the loops became detectable. A three-hour data set (00:00 UT–03:00 UT) taken by the AIA on board the *Solar Dynamics Observatory* (Lemen et al. 2012) was used for detailed analysis. The fan loops of interest are visible in both 171 and 193 Å, so we only use these two channels for study.

3. Results

3.1. Time Evolution of Intensity Oscillations

To derive the properties of the oscillations, we placed three artificial slices, S1, S2, and S3, along the fan loops as shown in Figure 2, at the locations where the intensity oscillations were clearly seen. We chose broad artificial slices in order to capture the longitudinal oscillations despite that they get displaced in the transverse direction due to interaction with the blast wave. It should be worth noting at this point that only one footpoint, close to the active region, of fan loops was clearly visible in 171 and 193 Å. The length of the artificial slices correspond to the distances along the fan loop up to which clear signatures of intensity oscillations were observed. Therefore, the length of the artificial slices may not be equal to the length of the fan loops. We discuss the estimation of the length of the fan loop in Section 3.3. For each of the three artificial slices, we generated a time–distance map, which henceforth will be termed as an x – t map throughout the Letter. Figure 3 represents the x – t maps for slices S1, S2, and S3 for 171 and 193 Å in the left, middle, and right panels, respectively. The signatures of intensity oscillations were clearer in AIA 171 Å as compared to AIA 193 Å because fan loops appeared more diffuse in AIA 193 Å. A possible reason for this is discussed in Section 3.4. The red vertical lines in Figure 3 represent the instances when blast

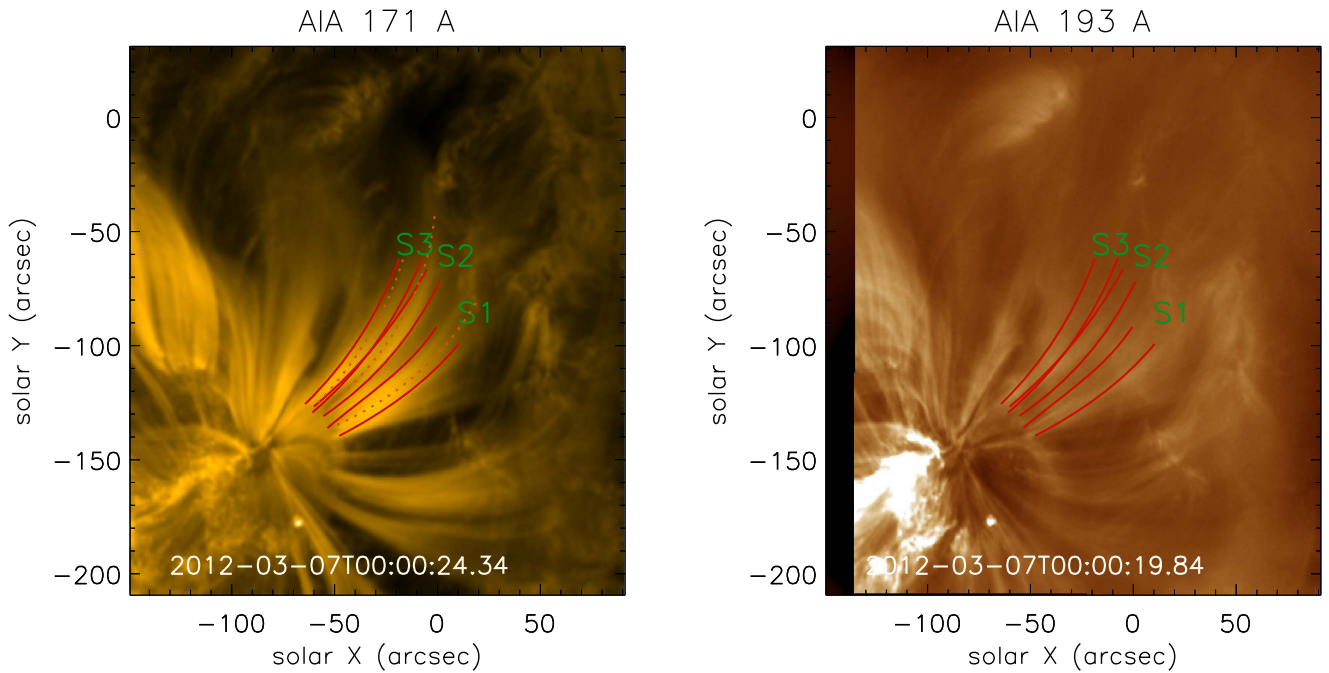


Figure 2. Left: AIA 171 Å image of the ROI shown in Figure 1. Three curved artificial broad slices, S1, S2, and S3, are overlaid in red which were used to generate the $x-t$ maps shown in Figure 3. The dotted curves in orange represent the length of the fan loops. Right: same as the left panel, but for AIA 193 Å. Animations corresponding to AIA 171 and 193 Å are available.

(Animations (a and b) of this figure are available.)

waves hit the fan loop system. We noticed that the second blast wave hit fan loops when the intensity oscillations driven by the first blast wave were still present.

Figure 3 shows that the intensity oscillations were out of phase at the two ends of the artificial slices as seen in the $x-t$ maps. The out-of-phase signature was clearly seen in both AIA 171 and 193 Å. It is clear from the Figure 3 that one reflection point (or antinode) of the oscillations was present near the one footpoint that is clearly visible in the intensity images, while the other antinode was present at the other end of the artificial slice, which may or may not be close to the other footpoint. From animations a and b of Figure 2, it is evident that the shape and appearance of the fan loops was changed after the second blast wave hit the fan loop system. Therefore, intensity oscillations were not clearly seen in $x-t$ maps after the second blast wave hit the fan loops.

Figure 4 shows the variation of intensity with time at different distances along the artificial slice S1. The Y -axis represents the relative intensity normalized to the local background. The two dashed vertical lines in red represent the instant of time when the blast wave hit fan loops. Since the blast wave hit the fan loops twice, we fitted the sinusoidal and damped sinusoidal curve separately at two different time intervals. The red curve represents the best-fit sinusoidal curve. We should point out that the damping of the oscillations were not seen clearly during the first period of observation, which may be due to the impact of the second blast wave. Thus, we did not fit a damped sinusoidal curve during the first time interval. However, we fitted a damped sinusoidal curve (shown in orange) in the second time interval and noticed the signature of damping at some locations along the fan loops (e.g., at 5 Mm). The intensity of oscillations became undetectable after 120 minutes because the shape and appearance of the fan loop changed (see animations a and b). The estimated average

period of the oscillation, P , and average damping times, τ , at the location of three slices, S1, S2, and S3 in 171 and 193 Å are listed in Table 1. Since only one oscillation was observed during the second interval, there were large uncertainties in the damping time. The quality factor (ratio of damping time by time period) estimated at the location of three slices is also listed in Table 1. These oscillations are weakly damped as compared to those reported earlier in hot coronal loops. A possible reason for weak damping is outlined in Section 4.

3.2. Variation of Amplitude of Intensity Oscillation

We noted that the relative amplitude (after normalizing with background intensity) of the intensity oscillations along S1 in 171 Å first decreased and then increased while moving from one end at S1 (close to one footpoint) to the other (may be close to another footpoint; see Figure 4). The variation can be seen clearly for both curves fitted at two separate time intervals shown in red and orange. Furthermore, the variation of the amplitude at different distances along S1, S2, and S3 in 171 and 193 Å is also shown in Figure 4. Systemic decrease and increase of the amplitude of oscillations, while moving from one end of the slice to another, was seen at the location of all slices. This signature clearly indicates the existence of an antinode near the footpoints of the fan loop.

3.3. Estimation of Loop Length and Velocity of the Oscillations

The footpoint of the fan loop that was away from the active region was distributed, and therefore not seen clearly in normal-intensity images of 171 or 193 Å. Thus, it was not straightforward to measure the length of the fan loops. Moreover, the shape and appearance of fan loops also changed with time (see animations a and b). To estimate the length, we chose the frames where the fan loops were best seen in

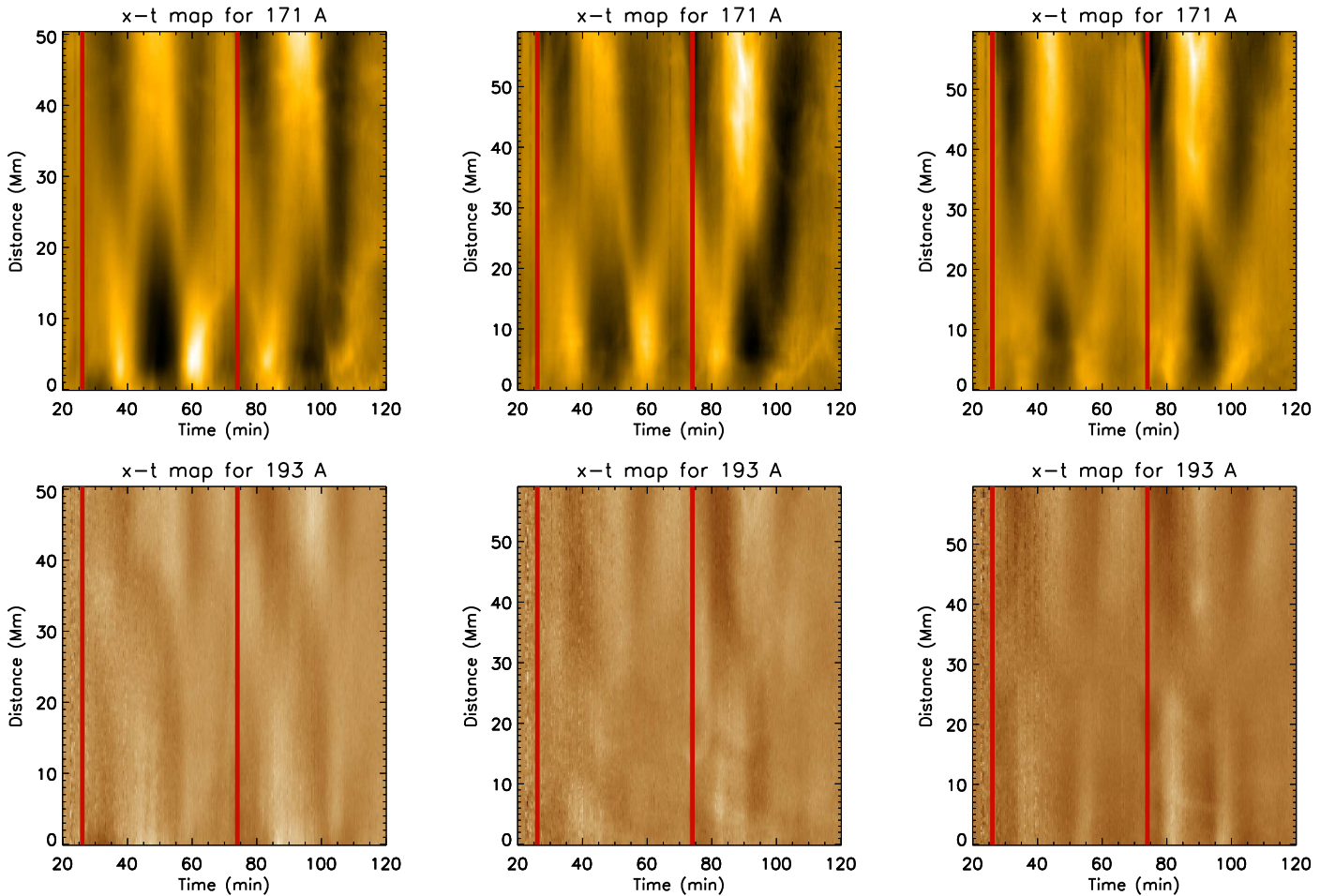


Figure 3. Time–distance ($x-t$) maps corresponding to slices S1, S2, and S3 as marked in Figure 2 are shown in the left, middle, and right panels, respectively. Two vertical red lines represent the time at which two blast waves impacted the fan loop system. The Y-axis represents the distance along the artificial slice.

normal-intensity images. We chose several points along the visible segment of the fan loops and interpolated a cubic spline between them. The length of the interpolated curve should be approximately equal to the projected length of the fan loops. The orange curves in Figure 2 are the fitted spline curves that represent the projected length of fan loops at the location of three artificial slices. We found the length of the fan loops at the locations of S1, S2, and S3 to be 62, 74, and 54 Mm, respectively (see Table 1). Note that the estimated length is the projected length in the plane of sky. Assuming the length of the fan loop is the same in 171 and 193 Å, we estimated the phase velocity of oscillations in 171 (193) Å to be 75 (85), 83 (101), and 65 (91) km s^{-1} at the locations of S1, S2, and S3, respectively. The phase velocity of oscillations, v , are comparable to the speed of sound in 171 and 193 Å.

3.4. Temperature and Density of the Fan Loop

We estimated the temperature and density of the fan loop using the automated differential emission measure technique as developed by Aschwanden et al. (2013). The temperature of the fan loops was found to be ~ 0.7 MK, which is much cooler than the hot loops as observed by hot SUMER lines (Wang et al. 2002) and in the AIA 94 Å channel (Wang et al. 2015). We also observed that the electron density decreased along the loop. Since the temperature of fan loops is low, they appear brighter in the 171 Å channel and diffuse in hotter channels

like 193 Å. We should point out that a fan loop may consist of several finer strands and we have not considered that scenario here.

4. Discussion and Conclusions

We observe intensity oscillations in a non-flaring fan loop system as seen in AIA 171 and 193 Å images. The intensity variations were out of phase close to two footpoints of fan loops, and the amplitude of the intensity oscillations varied along fan loops at the location of artificial slices. The amplitude of intensity oscillations first decreased and then increased while moving from one footpoint to another along the fan loop. It should be noted that it is difficult to identify the differences between standing and propagating waves without spectroscopic signatures. Recently, Yuan et al. (2015) have performed forward modeling of standing slow magnetoacoustic waves in flaring loops. They have reported that the variation of amplitude along the coronal loops is one of the signatures of the standing slow magnetoacoustic waves (see Figure 8 in Yuan et al. 2015). Moreover, a small phase shift in the intensity variations with time at different distances along fan loop corresponding to slice S1, as seen in Figure 4, can be due to the presence of standing slow oscillations (Taroyan et al. 2007; Taroyan & Bradshaw 2008). We estimated the time period of the oscillations to be ~ 27 minutes and the damping time to be ~ 45 minutes. We calculated the projected length of the fan

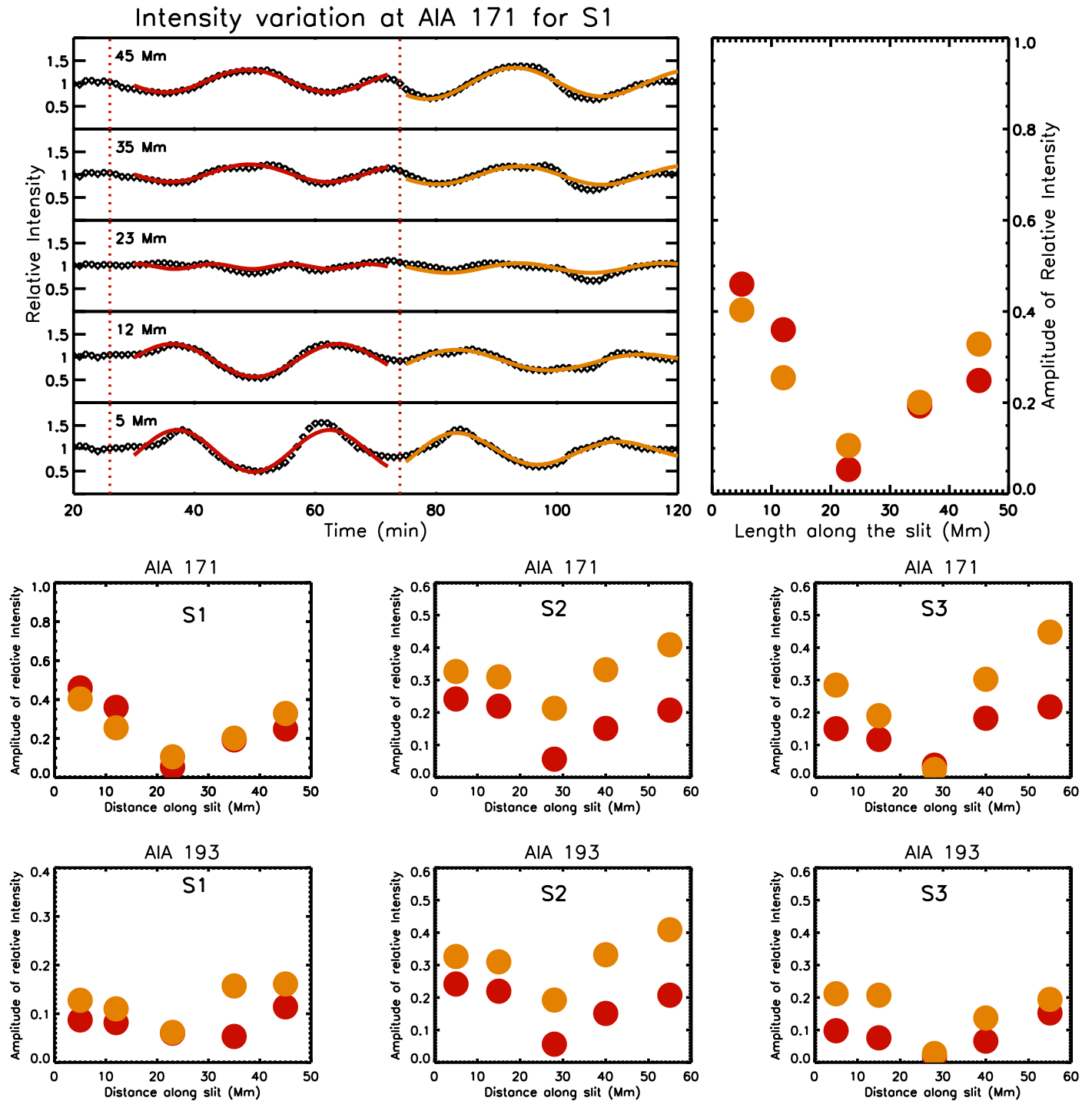


Figure 4. Top left: intensity variation after normalizing to the background intensity, at different distances along S1. Two vertical dashed lines represent the instances when the blast wave hit the fan loops system. Middle and bottom: variation of the amplitude of intensity oscillations for S1, S2, and S3 in 171 and 193 Å. Top right: same as the middle left panel.

loops and estimated that the velocity of oscillations are comparable to the velocity of sound in 171 and 193 Å. These signatures allow us to conclude that the observed oscillations are due to standing slow waves in coronal fan loops. The fan loops under study are associated with a sunspot. Yuan et al. (2011) reported the presence of long-period oscillations in the coronal diffused plasma near an active region. The oscillations observed in this study are different from those reported by Yuan et al. (2011) because the event under study was triggered by the energy impulse of flares, while Yuan et al. (2011)

studied the persistent leakage of long-period oscillations from the underneath sunspot.

It is worth mentioning that only one footpoint of fan loops was clearly seen in AIA 171 and 193 Å images. At this stage we can only conjecture two possible scenarios by which the reflection of the wave from the other end can happen. Either the antinode of the oscillations is present at the other footpoint, which is distributed and therefore not seen clearly in normal-intensity images, or the antinode could be present at the region of sharp density contrast close to the other end of the fan loop.

Table 1
Observational Parameters of Oscillations

Slice	AIA 171 Å					AIA 193 Å				
	P (minutes)	τ (minutes)	Q	l (Mm)	v (km s ⁻¹)	P (minutes)	τ (minutes)	Q	l (Mm)	v (km s ⁻¹)
S1	27.5 ± 1.8	40 ± 25	1.45	62	75	24.1 ± 5.4	37 ± 18	0.81	62	85
S2	29.6 ± 3.8	53 ± 25	1.79	74	83	24.4 ± 4.6	20 ± 10	1.53	74	101
S3	27.6 ± 4.7	42 ± 20	1.52	54	65	19.7 ± 1.7	42 ± 12	1.72	54	91

Note. P represents the period of oscillations; τ represents the damping time; Q is the quality factor, defined as the ratio of damping time and period of oscillations; l is the projected length of the fan loop at the location of the slice; and v is the velocity of the oscillations.





The region of sharp density change may have acted as a reflecting surface. These scenarios may be experimented on in future studies using computer simulations.

At most of the locations along the fan loops, oscillations are found to be undamped. The reason for the absence of damping at most of the locations is not clear to us; more observations of such events are required to reach conclusive views on the damping. However, at a few locations along the fan loop, we indeed noted weak damping. The oscillations at those locations are weakly damped as compared to those reported in Ofman & Wang (2002) and Wang et al. (2002, 2003b, 2015), where the damping time was comparable to the time period of the oscillations in hot and flaring coronal loops ($T > 6$ MK). One of the reasons for weak damping could be because the fan loops under study are not hot (~ 0.7 MK); thus, the thermal conduction may not be efficient enough. Since thermal conduction is one of the main mechanisms to damp slow waves, the oscillations were weakly damped in our study.

In summary, we found the signatures of standing slow magnetoacoustic waves in cool fan loops. In earlier studies, these oscillations were particularly observed in the hot coronal loops. To the best of our knowledge, this is the first report on the observational signatures of the existence of weakly damped standing oscillations in cool fan loops.

The authors thank the referee for valuable in-depth comments that helped to improve the manuscript.

ORCID iDs

V. Pant  <https://orcid.org/0000-0002-6954-2276>
A. Tiwari  <https://orcid.org/0000-0001-6021-8712>
D. Yuan  <https://orcid.org/0000-0002-9514-6402>
D. Banerjee  <https://orcid.org/0000-0003-4653-6823>

References

- Aschwanden, M. J., Boerner, P., Schrijver, C. J., & Malanushenko, A. 2013, *SoPh*, **283**, 5
- Bryans, P., McIntosh, S. W., De Moortel, I., & De Pontieu, B. 2016, *ApJL*, **829**, L18
- DeForest, C. E., & Gurman, J. B. 1998, *ApJL*, **501**, L217
- Fang, X., Yuan, D., Van Doorselaere, T., Keppens, R., & Xia, C. 2015, *ApJ*, **813**, 33
- Jiao, F., Xia, L., Li, B., et al. 2015, *ApJL*, **809**, L17
- Kumar, P., Innes, D. E., & Inhester, B. 2013, *ApJL*, **779**, L7
- Kumar, P., Nakariakov, V. M., & Cho, K.-S. 2015, *ApJ*, **804**, 4
- Lemen, J. R., Title, A. M., Akin, D. J., et al. 2012, *SoPh*, **275**, 17
- Mandal, S., Yuan, D., Fang, X., et al. 2016, *ApJ*, **828**, 72
- Ofman, L., Nakariakov, V. M., & DeForest, C. E. 1999, *ApJ*, **514**, 441
- Ofman, L., Romoli, M., Poletto, G., Noci, G., & Kohl, J. L. 1997, *ApJL*, **491**, L111
- Ofman, L., & Wang, T. 2002, *ApJL*, **580**, L85
- Pant, V., Dolla, L., Mazumder, R., et al. 2015, *ApJ*, **807**, 71
- Samanta, T., Pant, V., & Banerjee, D. 2015, *ApJL*, **815**, L16
- Taroyan, Y., & Bradshaw, S. 2008, *A&A*, **481**, 247
- Taroyan, Y., Erdélyi, R., Doyle, J. G., & Bradshaw, S. J. 2005, *A&A*, **438**, 713
- Taroyan, Y., Erdélyi, R., Wang, T. J., & Bradshaw, S. J. 2007, *ApJL*, **659**, L173
- Tsiklauri, D., Nakariakov, V. M., Arber, T. D., & Aschwanden, M. J. 2004, *A&A*, **422**, 351
- Wang, T. 2011, *SSRv*, **158**, 397
- Wang, T., Ofman, L., Sun, X., Provornikova, E., & Davila, J. M. 2015, *ApJL*, **811**, L13
- Wang, T., Solanki, S. K., Curdt, W., Innes, D. E., & Dammasch, I. E. 2002, *ApJL*, **574**, L101
- Wang, T. J., Solanki, S. K., Curdt, W., et al. 2003a, *A&A*, **406**, 1105
- Wang, T. J., Solanki, S. K., Innes, D. E., & Curdt, W. 2005, *A&A*, **435**, 753
- Wang, T. J., Solanki, S. K., Innes, D. E., Curdt, W., & Marsch, E. 2003b, *A&A*, **402**, L17
- Yuan, D., Nakariakov, V. M., Chorley, N., & Foullon, C. 2011, *A&A*, **533**, A116
- Yuan, D., Su, J., Jiao, F., & Walsh, R. W. 2016, *ApJS*, **224**, 30
- Yuan, D., Van Doorselaere, T., Banerjee, D., & Antolin, P. 2015, *ApJ*, **807**, 98